International Journal of Hydrogen Energy xxx (xxxx) 1–8

Contents lists available at ScienceDirect

International Journal of Hydrogen Energy

journal homepage: www.elsevier.com

Journal logo

Short Communication

In-situ dehydrogenation of lignin-based jet fuel: A novel and sustainable liquid organic hydrogen carrier

Andrew S. Lipton [a], Terak Ibrahim [b], William Schwartz [b], Rafal Gieleciak [c, **], Dequan Xiao [b, ***], Bin Yang [a, d, *]

[a] Environmental Molecular Sciences Laboratory, Pacific Northwest National Laboratory, Richland, WA, 99354, USA
[b] Center for Integrative Materials Discovery, Department of Chemistry and Chemical and Biomedical Engineering, University of New Haven, West Haven, CT, 06516, USA
[c] Natural Resources Canada, CanmetENERGY Devon, One Oil Patch Drive, Devon, AB, T9G 1A8, Canada
[d] Bioproducts, Sciences, and Engineering Laboratory, Department of Biological Systems Engineering, Washington State University, Richland, WA, 99354, USA

ARTICLE INFO

Suleyman I. Allakhverdiev

Keywords:
Hydrogen storage
Liquid organic hydrogen carriers
Sustainable aviation fuels
Lignin jet fuel
Cycloalkanes

ABSTRACT

A new and sustainable liquid organic hydrogen carrier, Lignin Jet Fuel-based Liquid Organic Hydrogen Carrier (LJF-HyC), has been discovered. This innovative LOHC is created from Lignin Jet Fuel (LJF) through dehydrogenation reactions. The process was carried out *in situ* using platinum nanoparticles supported on zeolite, resulting in a significant increase in aromatic carbon content. This increase indicates the successful formation of aromatic rings via C–H dissociation. *In-situ* Nuclear Magnetic Resonance (NMR) and gas chromatographic analyses revealed the formation of unsaturated and partially unsaturated compounds, including alkylbenzenes, tetralins, naphthalenes with double bond equivalence of 4–8, from six apparent reaction pathways, four of which can be major. The original LJF, consisting primarily of mono-, di-, and tricyclohexylalkanes (96 wt%), was converted to dehydrogenated products, constituting approximately 18.5 wt% of the LJF composition. These findings pave the way for developing sustainable hydrogen carriers derived from sustainable aviation fuels.

1. introduction

Hydrogen is a versatile energy carrier that supports the U.S. in achieving key strategic objectives, such as zero-emission mobility, sustainable energy integration, and industrial decarbonization [1–6]. Despite its potential, hydrogen's low density and highly explosive nature make storage and transportation technically challenging, inefficient, and costly. Liquid organic hydrogen carriers (LOHCs) have emerged as a promising solution to tackle these challenges. LOHC systems allow hydrogen to be chemically bound to a liquid carrier for safe and efficient storage and transportation, which can be easily released through catalytic dehydrogenation at the point of use [1,5,7]. The concept of LOHC technology facilitates efficient high-density hydrogen storage in an easy-to-handle sustainable aviation fuel (SAF). This approach offers promising opportunities for compatibility with existing infrastructure, economic viability for scalable production, and creating a synergistic system that enhances the efficiency, safety, and sustainability of both SAF and hydrogen technologies [8–11].

A patented Lignin-Based Jet Fuel (LJF) primarily consists of cycloalkane hydrocarbons, including alkyl-substituted mono-, bi-, and tricyclohexyl alkanes (Fig. 1) [12–15]. This LJF offers promising features such as high energy density, potential for reduced emissions, and favorable blending properties that align with drop-in fuel specifications [15–17]. A previous study suggests this pathway can generate LJF with a projected minimum selling price of \$2.87/gal when coupled with a cellulosic ethanol plant [18,19]. This technology enables the production of an aviation fuel/fuel blend stock with a high energy content, which may enhance fuel performance, improve fuel efficiency, reduce emissions, and lower costs. The LJF shows seal volume swell similar to traditional aromatics-containing jet fuels, potentially enabling the development of renewable jet fuels without aromatics [14,15]. It is known that some aromatic and heteroaromatic compounds are considered promising LOHCs due to their high hydrogen storage capacity and their ability to form stable and easily reversible chemical bonds with hydrogen [20,21]. In this study, the dehydrogenation of LJF into LJF-HyC re-

* Corresponding author. Environmental Molecular Sciences Laboratory, Pacific Northwest National Laboratory, Richland, WA, 99354, USA.
** Corresponding author.
*** Corresponding author.
E-mail addresses: rafal.gieleciak@nrcan-rncan.gc.ca (R. Gieleciak), DXiao@newhaven.edu (D. Xiao), bin.yang@wsu.edu (B. Yang).

https://doi.org/10.1016/j.ijhydene.2024.12.082
Received 18 October 2024; Received in revised form 25 November 2024; Accepted 5 December 2024
0360-3199/© 2022

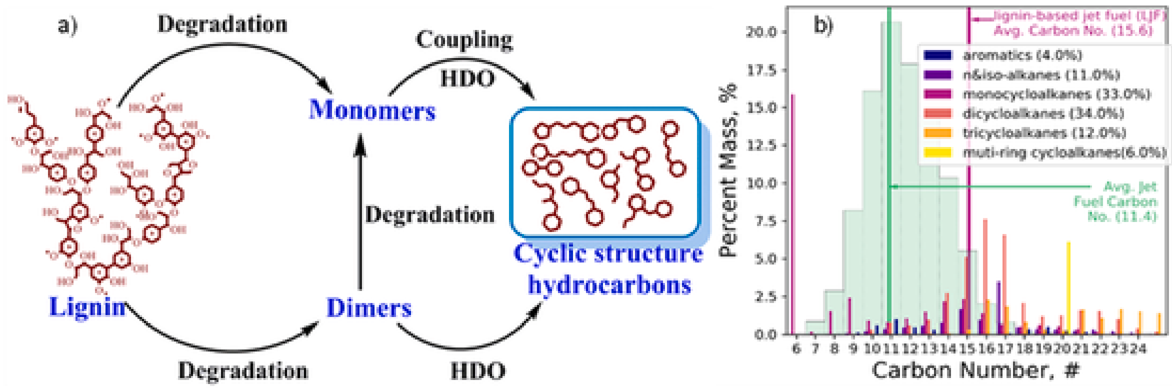

Fig. 1. a) Proposed LJF production pathways; b) Tier α hydrocarbon type analysis on neat LJF [14,15].

vealed a significant presence of unsaturated species, comprising approximately 18.5 wt% of the dehydrogenated LJF.

Pt-based catalysts (e.g., Pt nanoparticles and atomic clusters) have shown excellent performances for the dehydrogenation of linear alkanes [22–24] and cyclohexanes [25–27] due to their superior C–H activation ability. Various supports have been used for Pt-based catalysts, such as Al_2O_3 [26,28], zeolite [28], and graphene [29]. In addition, doping Pt with a second metal, such as Sn, Ga, Zn, Cu, Co, and Mn can lower the amount of Pt usage and even lead to improved catalytic activities [30,31]. In this work, we synthesized Pt nanoparticles (5–10 nm) supported on zeolite for the dehydrogenation of LJF.

This study presents an in-depth investigation of the dehydrogenation of lignin-based jet fuel using synthesized platinum nanoparticles supported on zeolite, employing *in situ* solid-state magic angle spinning (MAS) Nuclear Magnetic Resonance (NMR) spectroscopy. The resulting products were analyzed using two-dimensional gas chromatography with flame ionization detection (GC × GC-FID), GC × GC coupled with time-of-flight mass spectrometry (GC × GC-TOFMS), and GC coupled with vacuum ultraviolet detection (GC-VUV) to identify and semi-quantitatively measure the various classes of dehydrogenated chemicals. This fundamental understanding of the LJF dehydrogenation process could pave the way for the development of highly efficient LJF-HyC technologies. For instance, given the substantial variety of chemicals (e.g., several hundred) with similar structures and properties involved in the LJF feedstock and dehydrogenation products, optimal conditions (catalyst, temperature, and pressure) will be investigated to develop new LOHC technology based on LJF-HyC.

2. Material and methods

2.1. Catalyst preparation

A 1.0 wt% Pt/Zeolite catalyst was prepared by aqueous ion exchange using Tetraammineplatinum (II) chloride hydrate ($Pt(NH_3)_4Cl_2 \cdot xH_2O$), 99.99% purity) from Sigma-Aldrich as the Pt precursor. The zeolite support was also obtained from Sigma-Aldrich. A total of 0.1 g of the Pt precursor was dissolved in 120 mL of deionized water, under vigorous stirring, 5.7 g of Zeolite support was slurred into the solution and kept under stirring for 24 h. An adequate amount of 32% ammonia solution (from Sigma-Aldrich) was added to adjust the pH to the desired range of 6.5–7.5. The slurry was stirred overnight. The solid catalyst was collected using rotary vacuum filtration and then subjected to calcination in air at 400 °C for 6 h. Afterward, the catalyst was reduced under high-purity H_2 (10 mbar) and Ar (100 mbar) at 400 °C for 4 h.

The transmission electron microscopy (TEM) images and diffraction patterns were acquired using an FEI Tecnai F20 electron microscope operated at 200 kV. The corresponding X-ray energy dispersive spectroscopy (EDS) elemental mappings were performed on the same instrument using an Oxford X-MaxN TSR detector. The samples for electron microscopy analysis were prepared by directly depositing the ethanol-diluted sample suspension onto TEM grids coated with holey carbon film, without any additional treatments.

2.2. LJF sample preparation

An engineered Ru on HY zeolite catalyst was introduced into a Parr reactor as described in previous studies [32,33]. The reactor was purged with hydrogen gas three times to remove residual air, and the pressure was set to 4 MPa at room temperature. The reactor was then heated to 250 °C to initiate the reaction, with the reaction duration varied to optimize product yield. After the reaction, the reactor was rapidly cooled by immersion in cold water. The headspace gas was released and its volume measured using the water displacement method. All liquid and solid residues from the reactor were transferred to a centrifuge tube. Ethyl acetate was used to extract the organic phase from the reaction mixture, ensuring efficient separation of the target product. The extracted sample was dried using anhydrous sodium sulfate to remove residual water. Before proceeding with any further dehydrogenation reactions and analyses, a distillation was carried out using equipment specifically designed for performing ASTM D86 [34].

The hydrogenated liquid organic product was stored under an inert atmosphere to prevent oxidation. A portion of the organic phase was analyzed using GCxGC-TOFMS, GCxGC-FID, and GC-VUV to confirm the chemical composition and ensure the absence of significant impurities [14,15,32,35].

The LJF sample was prepared using a hydrodeoxygenation process established in prior studies [36]. An engineered Ru on HY zeolite catalyst was added to the Parr reactor [15,32]. The hydrogen pressure was set to 4 MPa at room temperature, after which the reactor was heated to a reaction temperature of 250 °C for 4 h. After reaction, all liquid and solid residues were transferred to a centrifuge tube, and the product was extracted from the reaction mixture using ethyl acetate. A sample was subsequently collected from the organic phase for further analysis [15,32,37].

2.3. In-situ Nuclear Magnetic Resonance

NMR experiments were conducted on ^{13}C utilizing a sealed MAS rotor in a wide-bore magnet (Oxford Instruments) operating at 11.7 T (500 MHz ^{1}H Larmor frequency) with a Direct Drive spectrometer from Agilent equipped with a home-built 5 mm HX probe (with ceramic spinning module from Revolution NMR), at Pacific Northwest National Laboratory, U.S.A. The ^{13}C chemical shifts are referenced to tetramethylsilane [$(CH_3)_4Si$] at 0.0 ppm by employing adamantane as a secondary external standard. The radio frequency (RF) fields for direct polarization (DP) involved a $\pi/2$ pulse of 5 μs for ^{13}C, while a ^{1}H decoupling field of 25 kHz was applied using the SPINAL-64 scheme [38].

The sealed rotors used were 5 mm o.d. cavern-style zirconia sleeves (Revolution NMR) modified to accommodate a Vespel double O-ring bushing. These modified rotors and seals, which have been previously described [39], allow the sample to maintain an internal pressure up to 22.5 MPa at 250 °C with a sample volume of 140 μL. The samples were sealed in the rotor at ambient pressure with a Kalrez® O-ring next to the sample area and a Viton™ O-ring on the outside of the bushing. The sample was spun to 4 kHz at 25 °C and the temperature was subsequently elevated to 150 °C, 170 °C, 190 °C, 210 °C, 230 °C, and 250 °C with ramped heating of 10 °C min^{-1} (sample temperatures were externally confirmed with ^{207}Pb NMR of lead nitrate). At each temperature, a DP ^{13}C spectrum was acquired. At 250 °C, ten consecutive 1-h ^{13}C spectra were collected, followed by an additional 10-h block of ^{13}C spectra. One final high S/N^{13}C spectrum was acquired before cooling back to 25 °C. Samples were prepared containing LJF (25.7 mg) and catalyst (22.0 mg). The products of the *in-situ* NMR reaction were then analyzed by gas chromatography.

2.4. Gas chromatography

The two-dimensional gas chromatography with time-of-flight mass spectrometry (GC × GC-TOFMS) analysis was performed using an Agilent 7890A GC and LECO Pegasus® 4D system. The first-dimension column was VF-5HT, 30 m × 0.32 mm × 0.1 μm (Agilent J&W), while the second-dimension column was BPX-50, 1.1 m × 0.1 mm × 0.1 μm (SGE Analytical Science). Samples were injected in split/splitless mode with an injection volume of 1 μL, using helium as the carrier gas at a flow rate of 1.2 mL/min. The oven temperature program began at 50 °C with an initial hold time of 2 min, ramped at 5 °C min^{-1} to 320 °C, and held for 2 min. The TOFMS was operated in electron ionization (EI) mode at 70 eV, scanning over a mass range of 40–500 m/z at an acquisition rate of 100 spectra/s. The transfer line was maintained at 350 °C, and the ion source at 200 °C.

The GC × GC with a flame ionization detector (FID) analysis was conducted using an Agilent 7890A GC with the same column configuration as described above. The injection and chromatographic conditions were the same as those used for the GC × GC-TOFMS analysis. The FID was maintained at a temperature of 350 °C, with hydrogen as the flame gas, air, and helium as the makeup gas. The concentration of product components detected after dehydrogenation is expressed as area percentage (Area%), as defined by Equation (1):

$$\text{Conc (Area\%)} = \frac{Area_{prod}}{\sum Area_{prod}} x\ 100 \tag{1}$$

where: $Area_{prod}$ is the GC × GC area of the respective compound.

The gas chromatography – vacuum ultraviolet detection (GC-VUV) system consisted of an Agilent 7890B GC connected to a VGA-101 VUV detector (VUV Analytics, Inc., TX, USA). Data analysis was performed using VUVision software. The specific operating conditions for the GC-VUV analysis are detailed in Table S1. After the analysis, the raw data files were exported from the VUVision software in CSV format and subsequently uploaded into the MATLAB (R2012b) environment for further processing and visualization.

3. results and discussion

3.1. NMR results

The dehydrogenation reaction was monitored using an *in-situ* NMR experiment, measuring ^{13}C spectra as the temperature increased from ambient to 250 °C. The monitoring continued with ^{13}C spectra measured at this elevated temperature in 1-h intervals. After the reaction, the spectrum was recorded again at 25 °C. Fig. 2 depicts the pre- and post-reaction ^{13}C spectra, clearly showing the formation of aromatics in the product spectrum, evident in the range of 120–140 ppm, that were absent initially. Also apparent in the figures are changes in the region

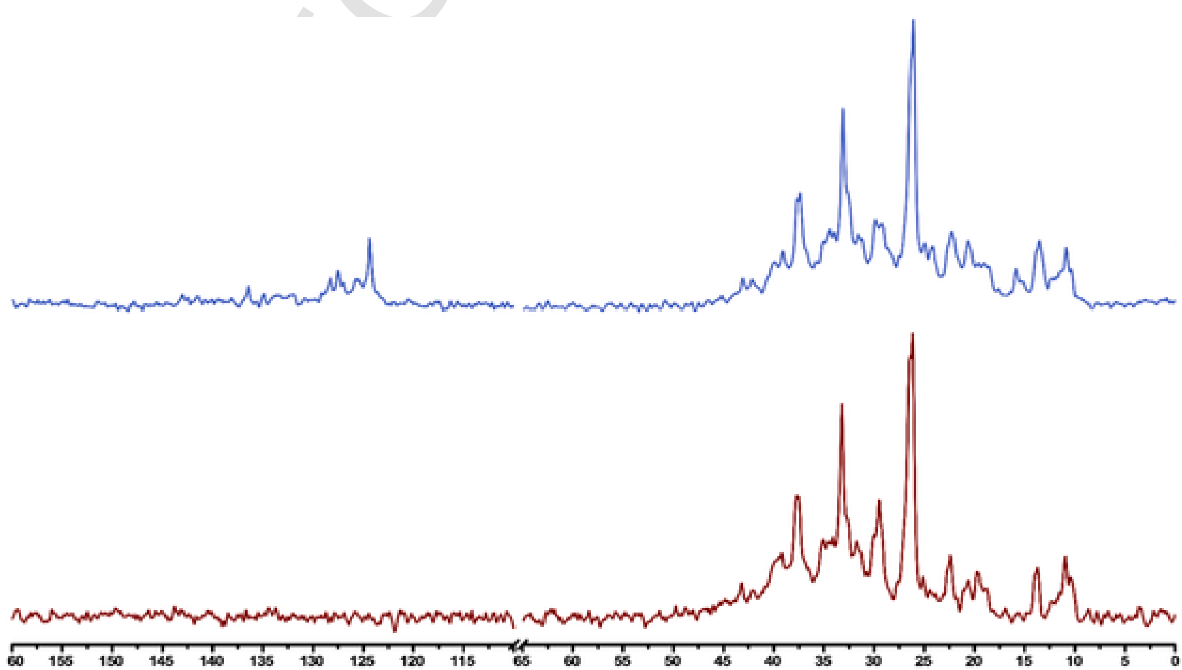

Fig. 2. The dehydrogenation reaction of LJF monitored with ^{13}C NMR where the bottom spectrum is LJF at the start and the top is the post reaction spectrum of LJF-HyC at 25 °C. The spectra are scaled to a uniform height.

from 10 to 25 ppm with the creation of new resonances in the product spectrum. The complete set of experimental ^{13}C NMR spectra are shown in Figure S1. The data in Figure S1 show that detection of the aromatic resonances does not begin until the temperature reaches 230 °C.

Fig. 3 plots the peak intensities at 124 ppm from the ^{13}C NMR spectra shown in Figure S1 for the reaction conducted at 250 °C.

Given that the LJF contains a mixture of reactants (various cycloalkanes), the signals at 124 ppm exhibit notable fluctuations throughout the reaction process. However, the trend line, represented as a red dashed curve in Fig. 3, indicates an increase in the aromatic carbon population over 12 h, followed by a subsequent decline. We envision that multiple dehydrogenation-rehydrogenation reactions could occur due to the presence of different reactants (R_i), as schematically described by Equation (1).

$$R_i \underset{+H}{\overset{-H}{\rightleftharpoons}} P_i \xrightarrow{+H} Q_i \qquad \text{Equation 1}$$

Dehydrogenation reactions lead to an increased concentration of aromatic carbons in product Pi. Concurrently, in the closed reaction system, the H_2 gas released during dehydrogenation does not escape but accumulates instead. This buildup of H_2 can potentially trigger rehydrogenation reactions. These rehydrogenation processes may cause a reverse reaction from P_i to R_i and could even generate different hydrogenated products, Q_i. The cumulative effect of multiple reactions (Equation (1)) might have resulted in the observed up-and-down behavior of the aromatic carbon population by the ^{13}C NMR measurement (Fig. 3).

3.2. Molecular transformations in LJF after dehydrogenation

The analysis of LJF before and after the dehydrogenation reaction involved various analytical techniques to determine their compositional profiles. These techniques included two-dimensional gas chromatography with flame ionization detection (GC × GC-FID), GC × GC coupled with time-of-flight mass spectrometry (GC × GC-TOFMS), and GC coupled with vacuum ultraviolet detection (GC-VUV).

The LJF is predominantly composed of alkanes and cycloalkanes, including mono-, di-, and tricyclohexylalkanes, which together account for approximately 96 wt% of its composition [14,15]. A detailed analysis indicates the following distribution: 11.8 wt% of n- and iso-alkanes, 20.3 wt% of monocyclohexylalkanes, 35.4 wt% of dicyclohexylalkanes,

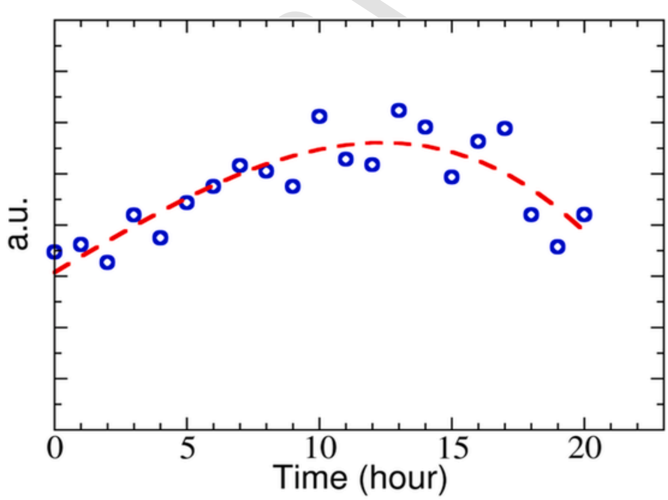

Fig. 3. Plot of the peak intensity at 124 ppm over a 20-h reaction period at 250 °C.

and 28.8 wt% of tricyclohexylalkanes. This complex hydrocarbon mixture is anticipated to undergo significant structural transformations during dehydrogenation reactions. In this section, the well-known analytical concept of double bond equivalence (DBE) will be used to elucidate the structural changes occurring during the dehydrogenation of LJF. DBE provides insight into the degree of unsaturation within molecules, a critical factor in understanding the outcomes of dehydrogenation processes, as it directly relates to the formation of double bonds and the resultant molecular structures. A higher DBE value indicates a higher degree of unsaturation, which may include the presence of double bonds, triple bonds, or rings within the molecular structure. DBE is calculated using the formula: $DBE = C - H/2 - X/2 + N/2 + 1$, where C is the number of carbon atoms, H is the number of hydrogen atoms, X is the number of halogen atoms, and N is the number of nitrogen atoms in the molecule [40]. This approach has been proven to be more appropriate for our study, especially considering that the compounds traditionally found in typical fossil fuel streams do not accurately represent the lignocellulosic materials being investigated. This methodological turn depicts the unique composition and properties of lignocellulosic materials, highlighting the need for tailored analytical approaches to truly understand their chemical composition and transformation processes, particularly in the context of aromatic hydrocarbon formation through dehydrogenation.

Fig. 4 presents GC × GC-FID chromatograms of LJF samples, identifying significant and most evident variations in peak position that suggest molecular transformations occurring after dehydrogenation. These variations are emphasized in Fig. 4b, where annotated circles highlight the differences. For example, the areas marked A1 – A4 on the chromatogram denote the regions that typically contain aromatic compounds i.e., alkylbenzenes, tetralins, naphthalenes, and phenanthrenes, respectively. This suggests the formation of partial or full aromatic hydrocarbons, likely due to the dehydrogenation reactions. We assigned DBE values for each region and found the following five classes of chemical species: C_nH_{2n-6} (DBE = 4), C_nH_{2n-8} (DBE = 5), C_nH_{2n-10} (DBE = 6), C_nH_{2n-12} (DBE = 7), and C_nH2_{n-14} (DBE = 8).

It is apparent that a significant number of peaks in the GC × GC chromatogram for the LJF sample post-dehydrogenation remain unchanged, suggesting that a substantial portion of these compounds remains largely unreactive in the closed system. Analysis with just the FID detector may not fully reveal the complexity of mixed chemicals, especially for highly coeluting compounds. This issue remains even at the highest chromatographic resolution, where partially unsaturated cycloalkane species may coelute with cycloalkanes. Consequently, to identify chemical structures of different DBE species before and after dehydrogenation, we applied the analysis of GC × GC-TOFMS.

This was achieved particularly by displaying selected ion chromatograms (SIC) with *m/z* values characteristic of a specific compound class. Figure S2 displays a selected series of SICs for the LJF sample, chosen to highlight the compositional changes occurring because of a dehydrogenation reaction. Each SIC chromatogram distinctively emphasizes the cumulative intensity of *m/z* values, indicative of unique hydrocarbon compound classes. These classes are identified by their DBE values and further described by a general molecular formula depicted in the lower right corner of Figure S2. Each pair of chromatograms within these examples contrast the samples' profiles before and after dehydrogenation, with the bottom chromatogram representing the sample prior to dehydrogenation and the top chromatogram illustrating the sample after dehydrogenation. This comparative approach not only highlights the specificity of the SIC technique in identifying compound classes within LJF samples but also demonstrates the significant impact of dehydrogenation on the molecular profiles of this sample.

Chemical structures from each of the five unsaturated hydrocarbon classes found in the LJF sample after dehydrogenation were identified using deconvoluted fragmentation mass spectral data and NIST library

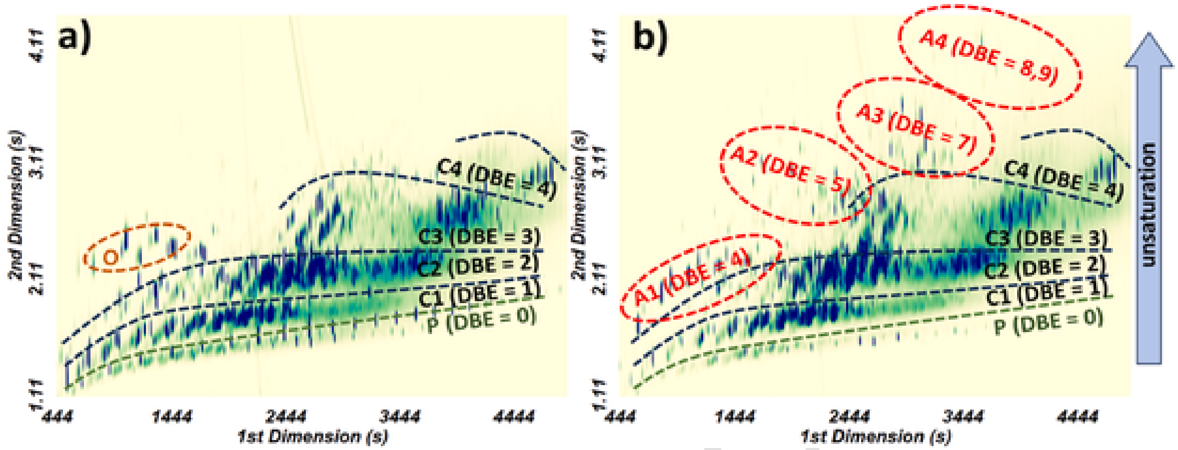

Fig. 4. GC × GC-FID chromatograms of LJF sample a) before and b) after dehydrogenation with depicted simplified elution regions of major hydrocarbon classes. The capital letters correspond to the hydrocarbon types: P) n-/iso-alkanes, C1) one-ring cyclic alkanes, C2) two-ring cyclic alkanes, C3) three-ring cyclic alkanes, C4) tetra-ring cyclic alkanes and steranes, O) oxygenates, A1) alkylbenzenes, A2) tetralins, A3) naphthalenes, A4) phenenthrenes/anthracenes. DBE (Double Bond Equivalent). Note that the peak color intensity indicates compound concentration – with dark blue indicating the highest abundance and light yellow representing the baseline.

searching. The compounds shown in Fig. 5 exhibit a high similarity factor (>750) between their mass spectra and the corresponding entries in the NIST library. In each panel, structures highlighted in red indicate the primary class structure compound for each group of compounds. These compounds illustrate the main molecular species for each DBE class in the dehydrogenated products. For example, for DBE = 4, the primary compounds have one fully unsaturated ring or two partially unsaturated rings. For DBE = 5, the compounds have one fully unsaturated ring and one fully saturated ring. For DBE = 6, the compounds have a fully unsaturated ring and a partially unsaturated ring with one double bond. For DBE = 7, the compounds have one naphthalene ring or a fully unsaturated ring plus a partially unsaturated ring with two double bonds. For DBE = 8, the compounds have two fully unsaturated rings.

A GC-VUV analysis was conducted to further verify the presence of unsaturated ring structures. This technique allows for the measurement of the VUV absorption of species after separation by gas chromatograph, which significantly aids in the spectrometric identification, classification, and quantification of compounds, such as saturates and aromatics. Moreover, in contrary to GC × GC-TOFMS analysis, GC-VUV provides the capability to distinguish cycloalkanes from alkenes. Typically, in GC-VUV analysis, analytes are identified by comparing their measured spectra with existing reference spectra in the library. This process of library searching, and the application of deconvolution algorithms form the foundation of ASTM D8071, ASTM D8267, and ASTM D8368 standards for analyzing the composition of gasoline, jet fuel, and diesel streams, respectively [41–43].

The GC-VUV data are shown as chromatograms of VUV absorption over elution time, see Fig. 6 (top panel), for the LJF samples. This en-

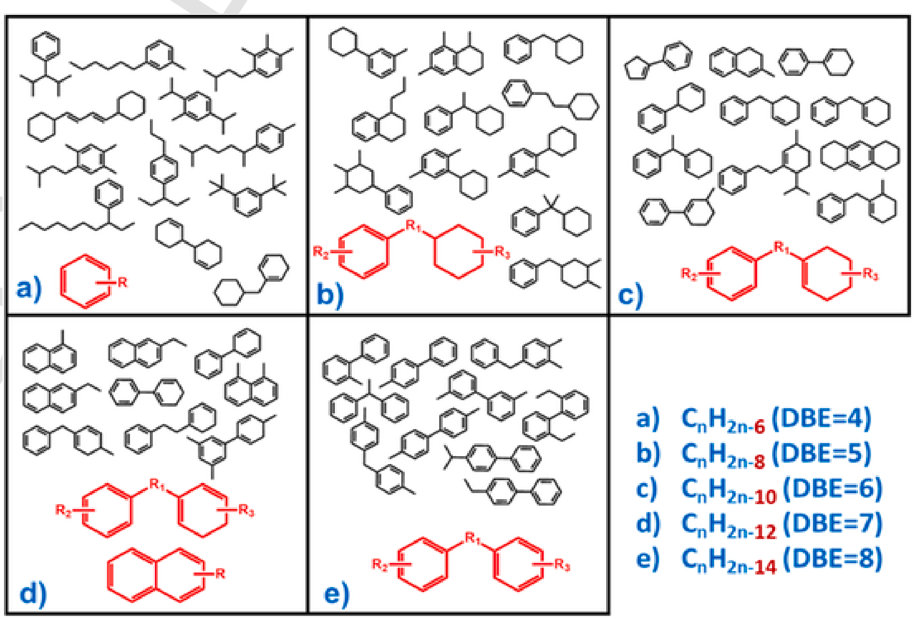

Fig. 5. Typical chemical structures of dehydrogenated LJF with DBE = 4 to 8, identified by GC × GC-TOFMS.

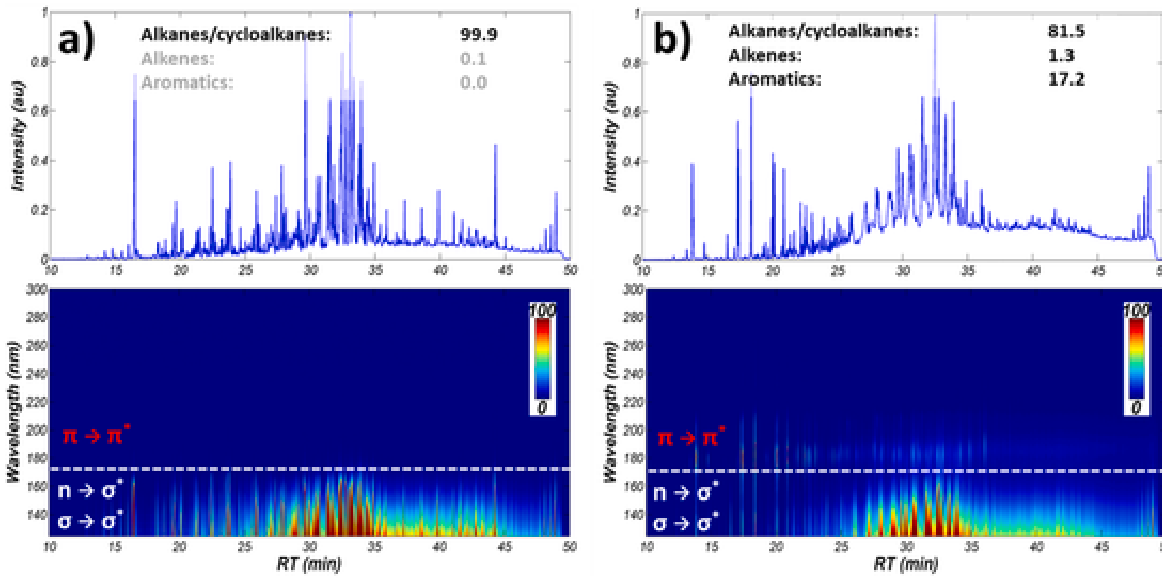

Fig. 6. (top) GC-VUV total VUV absorption chromatograms of LJF sample (a) before and (b) after dehydrogenation. (Bottom) GC × VUV chromatograms. In both, the x-axis represents GC elution time. In (bottom), y-axis represents the absorption wavelength spectrum, z-axis (indicated by color) denotes normalized intensity.

ables compound identification through unique chemical signatures and generates distinct absorption spectra, reflecting their chemical structures, as nearly all molecular compounds exhibit absorption in this region. Utilizing spectral data, GC-VUV data can be displayed as an image, with retention time and VUV wavelength on the x and y axes, respectively, and signal intensity color-coded [44]. This presentation method for LJF samples, before and after dehydrogenation, is demonstrated in the lower panel in Fig. 6.

Upon analyzing the GC-VUV data, distinct absorption trends are evident in LJF samples before and after the reaction, particularly in the $\pi \rightarrow \pi^*$ absorption region. Unique spectral features enable the differentiation of various hydrocarbon types. Saturates absorb strongly at $\lambda < 175$ nm and weakly at $\lambda > 175$ nm, while unsaturated species (alkenes and aromatics) absorb due to π-electron transitions. Alkenes absorb above and below 175 nm, influenced by molecular structure and geometry. Aromatics show strong absorption at $\lambda > 175$ nm and weak absorption at $\lambda < 175$ nm, with the absorption peak shifting to longer wavelengths as the number of aromatic rings increases.

Saturated and unsaturated compounds were semi-quantitatively analyzed using GC × GC and GC-VUV techniques. The analyses revealed a significant presence of unsaturated species in the LJF-HyC, comprising approximately 18.5 wt% of the dehydrogenated LJF composition. This notable proportion underscores the effective enrichment of unsaturated compounds alongside the dominant 81.5 wt% contribution of saturated species, as confirmed by both analytical methods.

3.3. Elucidation of reaction pathways

According to the *in-situ* NMR analysis and the results of GC × GC and GC-VUV, we deduced six typical or primary dehydrogenation pathways for the LJF-HyC formation, as shown in Fig. 7. The monocyclohexanes (C1) of LJF can be converted to fully unsaturated mono aromatics (A1). Chemical species containing decalin rings (C2F) in LJF can be converted to compounds with naphthalene rings (A2F). These two pathways can be major ones based on anticipated dehydrogenation mechanisms. There are four additional apparent reaction pathways for dicyclohexylalkanes (C2) in LJF-HyC. They can be converted to chemicals with a fully unsaturated ring plus another ring with 0–3 double bonds, i.e., A2D5, A2D6, A2D7, and A2D8, corresponding to DBE = 5 to 8, respectively. Based on 2D-GC peak intensities and dehydrogenation mechanism deduction, we envision that A2D6 and A2D7 may be the intermediates (in relatively small amounts) that can be converted into A2D8 given sufficient time. Thus, the pathways C2 to A2D5 and A2D8 can be the major ones. The dehydrogenation of tricyclohexylalka-

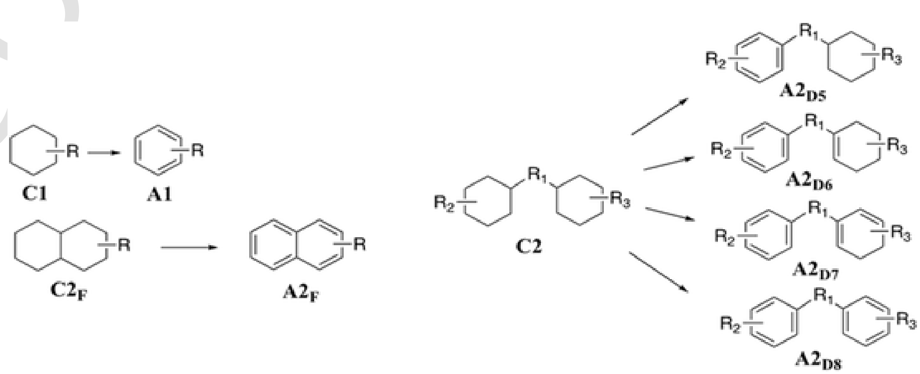

Fig. 7. Proposed reaction pathways during the dehydrogenation of LJF.

nes can lead to products with DBE > 8, which is not readily apparent as detected by the two-dimensional GC analysis. Thus, complete dehydrogenation of tricyclohexylalkanes is not predominant in the LJF, and the reaction pathways are not illustrated here.

4. conclusions

We demonstrated the LJF-HyC process via an *in-situ* dehydrogenation of LJF using Pt nanoparticles supported on zeolite. *In-situ* NMR analysis revealed that the dehydrogenation reactions initially show an exponential increase in aromatic carbon content, indicating the formation of aromatic rings following C–H dissociation. The rehydrognenation process was also observed to occur within this closed reaction system. The original LJF consists mainly of mono-, di-, and tricyclohexylalkanes, constituting approximately 96 wt%. Through GC × GC and GC-VUV analyses, the dehydrogenated products were identified as primarily containing five classes of compounds, with DBE values ranging from 4 to 8. GC × GC-TOFMS confirmed that these classes include among other alkylbenzenes, tetralins, and naphthalenes comprising approximately 18.5 wt% of the dehydrogenated LJF composition. Based on these findings, six apparent reaction pathways are proposed for the dehydrogenation of LJF to form LJF-HyC, where four of them can be the major pathways. This research advances the development of a novel and sustainable LJF-HyC technology.

CRediT authorship contribution statement

Andrew S. Lipton: Writing – review & editing, Writing – original draft, Validation, Supervision, Methodology, Investigation, Funding acquisition. **Terak Ibrahim:** Investigation. **William Schwartz:** Investigation. **Rafal Gieleciak:** Writing – review & editing, Writing – original draft, Validation, Supervision, Investigation, Funding acquisition. **Dequan Xiao:** Writing – review & editing, Writing – original draft, Validation, Project administration, Methodology, Funding acquisition, Conceptualization. **Bin Yang:** Writing – review & editing, Writing – original draft, Validation, Supervision, Resources, Project administration, Methodology, Investigation, Funding acquisition, Conceptualization.

Ethics approval and consent to participate

Not applicable.

Consent for publication

All the authors mutually consent for publication this manuscript and state that has not been previously published in another journal.

Data availability

The data supporting this study's findings are available from the corresponding authors (Drs Andrew Lipton, Rafal Gieleciak, Dequan Xiao, Bin Yang) upon reasonable.

Disclaimer

The views and opinions of the authors expressed herein do not necessarily state or reflect those of the United States Government or any agency thereof. Neither the United States Government nor any agency thereof, nor any of their employees, makes any warranty, expressed or implied, or assumes any legal liability or responsibility for the accuracy, completeness, or usefulness of any information, apparatus, product, or process disclosed, or represents that its use would not infringe privately owned rights.

Declaration of competing interest

The authors declare that they have no known competing financial interests or personal relationships that could have appeared to influence the work reported in this paper.

Acknowledgement

We are grateful for support from U.S. Department of Energy DOE-EERE Awards (DE-EE0011099 and DE-EE0009257) with the Bioproducts, Science & Engineering Laboratory and Department of Biological Systems Engineering at Washington State University. A portion of the research was performed on a project award from the Environmental Molecular Sciences Laboratory, a DOE Office of Science User Facility sponsored by the Biological and Environmental Research program under Contract No. DE-AC05-76RL01830. RG would like to acknowledge Natural Resources Canada and the government of Canada's interdepartmental program of energy research and development (PERD).

Appendix A. Supplementary data

Supplementary data to this article can be found online at https://doi.org/10.1016/j.ijhydene.2024.12.082.

References

[1] Dickson R, Akhtar M.S, Abbas A, Park E.D, Liu J. Global transportation of green hydrogen via liquid carriers: economic and environmental sustainability analysis, policy implications, and future directions. Green Chem 2022;24:8484–93.
[2] Teichmann D, Arlt W, Schluecker E, Wasserscheid P. Transport and storage of hydrogen via liquid organic hydrogen carrier (LOHC) systems. Wiley-VCH Verlag GmbH & Co. KGaA; 2016. p. 811.
[3] Ravi S.S, Aziz M. Clean hydrogen for mobility - quo vadis? Int J Hydrogen Energy 2022;47:20632–61.
[4] Preuster P, Papp C, Wasserscheid P. Liquid organic hydrogen carriers (LOHCs): toward a hydrogen-free hydrogen economy. Acc Chem Res 2017;50:74–85.
[5] Preuster P, Alekseev A, Wasserscheid P. Hydrogen storage technologies for future energy systems. Annu Rev Chem Biomol Eng 2017;8:445–71.
[6] Panigrahi P.K, Chandu B, Motapothula M.R, Puvvada N. Potential benefits, challenges and perspectives of various methods and materials used for hydrogen storage. Energy Fuel 2024;38:2630–53.
[7] Niermann M, Beckendorff A, Kaltschmitt M, Bonhoff K. Liquid organic hydrogen carrier (LOHC) – assessment based on chemical and economic properties. Int J Hydrogen Energy 2019;44:6631–54.
[8] Teichmann D, Arlt W, Wasserscheid P. Liquid Organic Hydrogen Carriers as an efficient vector for the transport and storage of renewable energy. Int J Hydrogen Energy 2012;37:18118–32.
[9] Tountas A.A, Ozin G.A, Sain M.M. Choosing a liquid hydrogen carrier for sustainable transportation. Sustain Energy Fuels 2024.
[10] Aakko-Saksa P.T, Cook C, Kiviaho J, Repo T. Liquid organic hydrogen carriers for transportation and storing of renewable energy – review and discussion. J Power Sources 2018;396:803–23.
[11] Ansell P.J. Review of sustainable energy carriers for aviation: benefits, challenges, and future viability. Prog Aero Sci 2023;141:100919.
[12] Yang B, Laskar D.D. Apparatus and process for preparing reactive lignin with high yield from plant biomass for production of fuels and chemicals. Washington State University; 2015.
[13] Yang B, Wang H. Hydrodeoxygenation of lignin to hydrocarbons using bimetallic catalysts. Washington State University; 2018.
[14] Ruan H, Qin Y, Heyne J, Gieleciak R, Feng M, Yang B. Chemical compositions and properties of lignin-based jet fuel range hydrocarbons. Fuel 2019;256:115947.
[15] Yang Z, Xu Z, Feng M, Cort J.R, Gieleciak R, Heyne J, et al. Lignin-based jet fuel and its blending effect with conventional jet fuel. Fuel 2022;321:124040.
[16] Laskar D.D, Yang B, Wang H, Lee J. Pathways for biomass-derived lignin to hydrocarbon fuels. Biofuels, Bioprod Biorefin 2013;7:602–26.
[17] Wandelt S, Blom H, Krömer M.M, Li D, Mitici M, Ryley T, et al. DESIGN and be SMART: eleven engineering challenges to achieve sustainable air transportation under safety assurance in the year 2050. J Air Trans Res Soc 2024;100045.
[18] Shen R, Tao L, Yang B. Techno-economic analysis of jet-fuel production from biorefinery waste lignin. Biofuels, Bioprod Biorefin 2019;13:486–501.
[19] Zhang L, Butler T.L, Yang* B. Recent trends, opportunities and challenges of sustainable aviation fuel. Green Energy Sustain: Strat Global Ind 2020;85–110.
[20] Jorschick H, Preuster P, Boesmann A, Wasserscheid P. Hydrogenation of aromatic and heteroaromatic compounds - a key process for future logistics of green hydrogen using liquid organic hydrogen carrier systems. Sustain Energy Fuels 2021;5:1311–46.
[21] Samoilov V.O, Sultanova M.U, Borisov R.S, Lavrent'ev V.M, Ramazanov D.N, Egazar'yants S.V, et al. The production of a liquid organic hydrogen carrier (LOHC)

and jet fuel fractions by hydroprocessing of pyrolysis fuel oil (PFO). Int J Hydrogen Energy 2024;49:1386–400.
[22] Cao R, Zhang M.-Q, Hu C, Xiao D, Wang M, Ma D. Catalytic oxidation of polystyrene to aromatic oxygenates over a graphitic carbon nitride catalyst. Nat Commun 2022;13:4809.
[23] Liu L, Meira D.M, Arenal R, Concepcion P, Puga A.V, Corma A. Determination of the evolution of heterogeneous single metal atoms and nanoclusters under reaction conditions: which are the working catalytic sites? ACS Catal 2019;9:10626–39.
[24] Zhang W, Wang H, Jiang J, Sui Z, Zhu Y, Chen D, et al. Size dependence of Pt catalysts for propane dehydrogenation: from atomically dispersed to nanoparticles. ACS Catal 2020;10:12932–42.
[25] Cromwell D.K, Vasudevan P.T, Pawelec B, Fierro J.L.G. Enhanced methylcyclohexane dehydrogenation to toluene over Ir/USY catalyst. Catal Today 2016;259:119–29.
[26] Lei P, Zhang J, Shen W, Zhong M, Guo S. Boosting the catalytic performance of Ru nanoparticles in the cleavage of β-O-4 linkages in lignin by doping Mo. Green Chem 2024;26:6616–24.
[27] Deng Y, Guo Y, Jia Z, Liu J.-C, Guo J, Cai X, et al. Few-atom Pt ensembles enable efficient catalytic cyclohexane dehydrogenation for hydrogen production. J Am Chem Soc 2022;144:3535–42.
[28] Maldonado-Hódar F.J, Ribeiro M.F, Silva J.M, Antunes A.P, Ribeiro F.R. Aromatization ofn-heptane on Pt/alkali or alkali-earth exchanged beta zeolite catalysts: catalyst deactivation and regeneration. J Catal 1998;178:1–13.
[29] Brodt M, Mueller K, Kerres J, Katsounaros I, Mayrhofer K, Preuster P, et al. The 2-propanol fuel cell: a review from the perspective of a hydrogen energy economy. Energy Technol 2021;9:2100164.
[30] Bao H, Sagues W.J, Wang Y, Peng W, Zhang L, Yang S, et al. Depolymerization of lignin into monophenolics by ferrous/persulfate reagent under mild conditions. ChemSusChem 2020;13:6582–93.
[31] Kobayashi S, Kaneko S, Ohshima M-a, Kurokawa H, Miura H. Effect of iron oxide on isobutane dehydrogenation over Pt/Fe2O3-Al2O3 catalyst. Appl Catal Gen 2012;417–418:306–12.
[32] Kumar A, Kumar A, Santosa D.M, Wang H, Zuo P, Wang C, et al. Engineered Ru on HY zeolite catalyst for continuous and selective hydrodeoxygenation of lignin phenolics to cycloalkanes under moderate conditions. Appl Catal Gen 2024;676:119649.
[33] Kumar A, Bell D.C, Yang Z, Heyne J, Santosa D.M, Wang H, et al. A simultaneous depolymerization and hydrodeoxygenation process to produce lignin-based jet fuel in continuous flow reactor. Fuel Process Technol 2024;263:108129.
[34] International A. ASTM D86-16a. Standard test method for distillation of petroleum products and liquid fuels at atmospheric pressure. 2016.
[35] Ruan H, Xu Z, Kumar A, Feng M, Lipton A.S, Walter E.D, et al. Elucidating the reaction pathways of veratrylglycero-β-guaiacyl ether degradation over metal-free solid acid catalyst with hydrogen. ChemSusChem 2023;16:e202202001.
[36] Wang H, Ruan H, Pei H, Wang H, Chen X, Tucker M.P, et al. Biomass-derived lignin to jet fuel range hydrocarbons via aqueous phase hydrodeoxygenation. Green Chem 2015;17:5131–5.
[37] Scanlon J.T, Willis D.E. Calculation of flame ionization detector relative response factors using the effective carbon number concept. J Chromatogr Sci 1985;23:333–40.
[38] Fung B, Khitrin A, Ermolaev K. An improved broadband decoupling sequence for liquid crystals and solids. J Magn Reson 2000;142:97–101.
[39] Walter E.D, Qi L, Chamas A, Mehta H.S, Sears J.A, Scott S.L, et al. Operando MAS NMR reaction studies at high temperatures and pressures. J Phys Chem C 2018;122:8209–15.
[40] Dayringer H.E, McLafferty F.W. Computer-aided interpretation of mass spectra. STIRS prediction of rings-plus-double-bonds values. Org Mass Spectrom 1977;12:53–4.
[41] Weber B.M, Walsh P, Harynuk J.J. Determination of hydrocarbon group-type of diesel fuels by gas chromatography with vacuum ultraviolet detection. Anal Chem 2016;88:5809–17.
[42] Schenk J, Mao J.X, Smuts J, Walsh P, Kroll P, Schug K.A. Analysis and deconvolution of dimethylnaphthalene isomers using gas chromatography vacuum ultraviolet spectroscopy and theoretical computations. Anal Chim Acta 2016;945:1–8.
[43] Gröger T, Gruber B, Harrison D, Saraji-Bozorgzad M, Mthembu M, Sutherland A, et al. A vacuum ultraviolet absorption array spectrometer as a selective detector for comprehensive two-dimensional gas chromatography: concept and first results. Anal Chem 2016;88:3031–9.
[44] Wang F.C.-Y. GC × VUV study of diesel: a two-dimensional separation approach. Energy Fuel 2020;34:1432–7.